Journal

Electrical Properties of Nb-, Ga-, and Y-Substituted Nanocrystalline Anatase TiO$_2$ Prepared by Hydrothermal Synthesis

E. Mitchell Hopper,[‡,†] Frédéric Sauvage,[§,¶,‖] Aravind Kumar Chandiran,[§] Michael Grätzel,[§] Kenneth R. Poeppelmeier,[‖] and Thomas O. Mason[‡]

[‡]Department of Materials Science and Engineering, Northwestern University, Evanston, IL 60208

[§]Laboratory of Photonics and Interfaces, Institute of Chemistry and Chemical Engineering, Swiss Federal Institute of Technology (EPFL), Station 6, CH 1015 Lausanne, Switzerland

[¶]Laboratoire de Réactivité et Chimie des Solides, Université de Picardie Jules Verne, CNRS UMR6007, 33 rue Saint-Leu, F-80039 Amiens Cedex, France

[‖]Department of Chemistry, Northwestern University, Evanston, IL 60208

Nanocrystalline anatase titanium dioxide powders were produced by a hydrothermal synthesis route in pure form and substituted with trivalent Ga^{3+} and Y^{3+} or pentavalent Nb^{5+} with the intention of creating acceptor or donor states, respectively. The electrical conductivity of each powder was measured using the powder-solution-composite (PSC) method. The conductivity increased with the addition of Nb^{5+} from 3×10^{-3} S/cm to 10×10^{-3} S/cm in as-prepared powders, and from 0.3×10^{-3} S/cm to 0.9×10^{-3} S/cm in heat-treated powders (520°C, 1 h). In contrast, substitution with Ga^{3+} and Y^{3+} had no measureable effect on the material's conductivity. The lack of change with the addition of Ga^{3+} and Y^{3+}, and relatively small increase upon Nb^{5+} addition is attributed to ionic compensation owing to the highly oxidizing nature of hydrothermal synthesis.

I. Introduction

THE anatase polymorph of TiO$_2$ is of considerable interest as a photocatalyst for water splitting and for self-cleaning coatings,[1] and is also of interest as a transparent conducting oxide and as a core component in optoelectronic devices such as dye-sensitized solar cells (DSSCs).[2–4] This interest exists, in part, owing to its $3d^0$ electronic configuration and the corresponding tunability of its optical band gap and electronic properties by introducing electronic defects.[2] We have recently shown that the introduction of electronic point defects in TiO$_2$ is an effective way to improve the charge collection and power conversion efficiencies in dye-sensitized and PbS-heterojunction solar cells[3,5] and eliminates the need for TiCl$_4$-based post treatments.[6,7] The role of the TiO$_2$ in these devices is crucial because it controls the light harvesting and confinement properties of the cell, in addition to preventing charge recombination and promoting charge transport toward the anode. These last two parameters are major factors in determining the charge collection efficiency.[8]

One very important technique used to improve the performance of DSSCs is aliovalent substitution of the TiO$_2$ with elements of different valence states. This allows the optoelectronic properties of the TiO$_2$ to be tailored by, for example, changing the carrier concentration[2] or shifting the absorption edge nearer to or farther from the visible range.[9–11] The donor dopant that has received the most attention in recent years is Nb^{5+}, which is attractive because of its similar ionic radius (0.64 Å vs 0.605 Å for Ti^{4+})[12] and ability to form strongly hybridized 4d orbitals with the 3d orbitals of Ti^{4+}.[13] Nb-doped TiO$_2$ has shown excellent performance as a transparent conducting oxide owing to its high conductivity in thin film form.[2] Acceptor dopants like Ga^{3+} and Y^{3+} are also of interest because they are known to improve the photocatalytic activity of TiO$_2$ without adversely affecting the band gap.[14–16]

In our previous work,[3,5] cell performance had been improved by substituting the Ti^{4+} site with either Ga^{3+}, Y^{3+}, or Nb^{5+}. These substitutions have been shown to affect the particle morphology, optical band gap, and the extent and type of trap states below the conduction band, all of which affect the performance of a DSSC.[17–19] However, little is known about their effect on the electrical conductivity of the powder. This effect is important to understand because it could explain the improvement in cell performance attributed to increased carrier lifetimes. In this work, we have employed the powder-solution-composite (PSC) method to examine the electrical conductivity of the best-performing powders used in DSSCs, made from precursors containing 0.5% and 1% Nb^{5+}, 1% Ga^{3+}, and 1% Y^{3+}, and compare them with pure TiO$_2$.

II. Experimental Procedure

Powders were made by adding 0.2 moles (12 g) of acetic acid (Sigma-Aldrich, Buchs, Switzerland) to 0.2 moles (58.6 g) of titanium isopropoxide (97%; Aldrich) under constant stirring. Nb^{5+} was added in the form of niobium pentachloride (99.9%; Aldrich), and Ga^{3+} and Y^{3+} were introduced as gallium nitrate (99.9%, Aldrich) and yttrium chloride (99.9%; Aldrich), respectively. This precursor was added drop-wise to the acetic acid/titanium isopropoxide solution to achieve the desired cation ratio (Nb, Ga, or Y to Ti). The product was then transferred into a conical flask containing 350 mL of water, which was vigorously stirred for 1 h to allow the hydrolysis reaction to complete. After the reactants were hydrolyzed, 4 mL of concentrated nitric acid (65%) was added and the solution was heated to 78°C for 90 min to peptize the particles. The solution was then concentrated to 150 g using a rotary evaporator and sealed within a Teflon-Parr pressure vessel (250 mL volume), which was heated in an autoclave at 250°C for 12 h. After cooling to room temperature, 1 mL of concentrated HNO$_3$ was added to the

colloidal solution and the solution was sonicated for 2 min. The sonication process was repeated three times with alternate stirring to homogeneously disperse the particles. The powder was recovered by centrifugation and dried at 50°C for 60 min. Samples of each powder also underwent an additional thermal treatment at 520°C for 1 h to mimic a processing step typically used in DSSC preparation prior to sensitization.

Phase purity and lattice parameter changes were analyzed using powder XRD with a Bruker D8 Discover diffractometer (Bruker, Karlsruhe, Germany) using a CuK_α source. For these measurements, powders were prepared with a range of initial Nb^{5+}, Ga^{3+}, and Y^{3+} concentrations. Energy-dispersive X-ray (EDX) spectroscopy measurements using an FEI XLF30-FEG scanning electron microscope (FEI, Eindhoven, the Netherlands) were performed on these samples to accurately measure the concentration of the substituting species. The spectrum simulation used to determine the compositions considered an active cross-section that depends on the energy dispersion and a fixed parameter that takes sample roughness into account. The valence state of the cations, as well as their concentrations, were investigated using X-ray photoelectron spectroscopy (XPS/ESCA KRATOS AXIS ULTRA, Kratos, Manchester, U.K.) using AlK_α radiation (1486.3 eV).

The conductivity of the powders was measured using the PSC method, which involves comparing the AC impedance response of liquid solutions with known conductivity to those of slurries containing both solution and powder.[20] Aqueous NaCl solutions were prepared with concentrations ranging from 5×10^{-4} M (8.0×10^{-5} S/cm) to 1 M (9.5×10^{-2} S/cm). Each solution was mixed with approximately 0.06 g of powder and compressed in a polyethylene tube (4.7-mm inner diameter) between two stainless steel plugs to achieve a powder volume fraction of 0.3–0.4, with an interelectrode distance of approximately 4 mm. The AC impedance responses of the solutions and slurries were measured by an HP4192A impedance analyzer (Agilent Technologies, Santa Clara, CA), to which the steel electrodes were connected by alligator clips attached to coaxial cables. A sinusoidal oscillating voltage amplitude of 1 V was used over the frequency range 10^1–10^7 Hz.

III. Results and Discussion

The composition of each sample as measured by EDX is presented in Table I in comparison to the molar ratio of the dopant to Ti in the precursor solution. The solubility of Y was very low compared to that of Ga and Nb, which is consistent with previous reports[21] and is expected based on the large ionic radius mismatch between Y^{3+} (0.90 Å) and Ti^{4+} (0.605 Å).[12] As in previous experiments,[3] XPS measurements showed that a small amount of Ti existed as Ti^{3+} in the as-prepared Nb-substituted powders. However, the Ti^{3+} signal disappeared after the heat treatment, indicating that all the Ti was present as Ti^{4+}, and the use of trivalent dopants (Ga, Y) resulted in no Ti^{3+} signal at any point.

XRD patterns confirmed the crystallization of the anatase polymorph in all samples without showing the presence of secondary phases resulting from the addition of Nb^{5+},

Ga^{3+}, or Y^{3+}, in agreement with Refs. 3 and 5. Also in accordance with these reports, a small amount of the rutile polymorph (<2%) was present in the pure TiO₂ and trivalent-substituted samples, owing to the acidity of the precursor solution (pH ≈ 1). This synthesis route is routinely used for DSSCs because the acidic medium prevents the formation of aggregated particles. The incorporation of niobium has been reported to increase the activation energy for the anatase-to-rutile transition, thus stabilizing the anatase crystal structure,[22] as observed in the current experiment.

The lattice parameters of each sample were determined using FullProf software (J. Rodríguez-Carvajal, Grenoble, France) in full pattern matching mode for samples containing Ga and Y, and following the Rietveld method for those with Nb. The lattice parameters increased with increasing degrees of substitution (Fig. 1) for all three dopants, and the calculated cell volumes increase steadily with substitution. These results confirm the solubility of all three species—Nb^{5+}, Ga^{3+}, and Y^{3+}—in the TiO₂ matrix.

To obtain the solution and composite conductivities, the impedance results were plotted using the Nyquist representation (negative imaginary impedance versus real impedance), in which each component of the system (e.g., electrode, solution, or composite) is represented by a semicircular arc. The real axis corresponds to resistance and the imaginary axis represents capacitance (negative values) or inductance (positive values). All samples exhibited two semicircular arcs, one at low frequencies attributed to the electrodes and a high-frequency arc representing the behavior
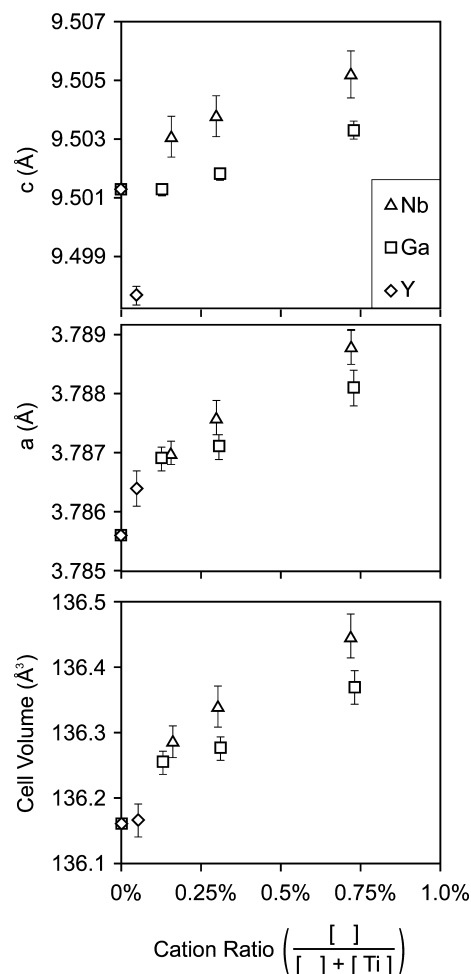
Fig. 1. Variation of lattice parameters and cell volume measured for TiO₂ powders with substitutional Nb (triangles), Ga (squares), and Y (diamonds). The cation ratios of the powders were measured using EDX.

Table I. Concentrations of Substitutional Elements on a Cation Basis Measured Using EDX for Each Powder Composition, Compared to the Ratio Introduced as Precursors During Synthesis

Dopant concentration introduced as precursor (molar% versus Ti)	0.5%	1.0%	2.0%
Nb concentration in powder	0.32%	0.62%	1.44%
Ga concentration in powder	0.13%	0.31%	0.72%
Y concentration in powder	<0.05%	<0.05%	≈0.05%

of the sample. The relative sizes of the solution and composite arcs reflect the progression from a solution-dominated composite [for high-conductivity solutions, Fig. 2(a)] to a composite containing powder that is more conductive than the solution [at low solution conductivity, Fig. 2(b)]. It should be stressed that although the equivalent circuit model of Fig. 3 (discussed below) can be used to fit the acquired AC-IS spectra, as demonstrated by the solid curves through the solution and composite arcs in Fig. 2, the only parameter required for PSC analysis is the resistance of the sample, taken to be the intersection of both arcs (sample and electrode) with the real impedance axis. Note that the leftmost (high-frequency) arcs appear incomplete because they extend beyond the frequency range of the impedance analyzer. In addition, the arcs observed in the current experiment were depressed rather than being complete semicircles, which was accounted for by modeling with constant phase elements in place of capacitor elements as discussed by Ingram, *et al.*[20]

The change in relative positions of the composite and solution arcs in Fig. 2 can be understood by analysis of the equivalent circuit established for the PSC system (Fig. 3). Electrical components of the system are represented by resistor-capacitor (RC) elements, and in Fig. 3 s represents the solution, c represents the powder-solution interface, and e represents the electrodes. The (R_sC_s) element represents the solution path itself, and $(R_s'C_s')$ represents current flowing around particles when they are more insulating than the solution. $(R_s''C_s'')$ represents current bunching between particles at the other extreme, when the powders are more conductive than the solution. Because there are parallel paths describing current traveling through the solution only, through both solution and particles, and directly from particle to particle (the $R_{percolation}$ path), current will tend to flow through whichever path has the lowest resistance. Note that $R_{percolation}$ differs from R_{powder} in that it accounts for spreading resistance encountered at particle-particle contact points. The resistance of the solution affects both the "solution" and "composite" paths, so when the solution is highly conductive these paths will dominate the impedance response of the composite. When the solution is very resistive, current will prefer to travel through the "composite" and "percolation" paths.[20]

The relationship between the conductivities of the composite slurries and their corresponding solutions can be visualized by plotting $\log(\sigma_{composite})$ as a function of $\log(\sigma_{solution})$, which were calculated from the corresponding resistances based on
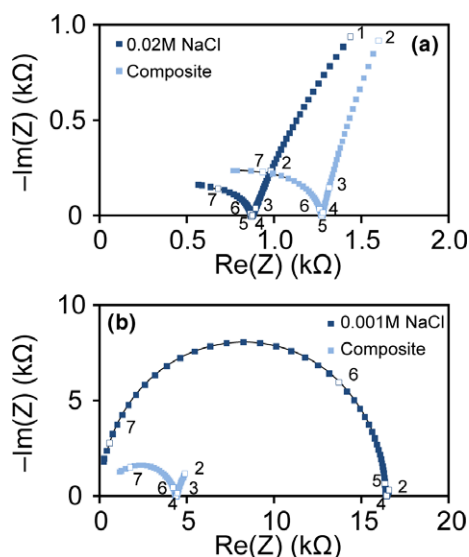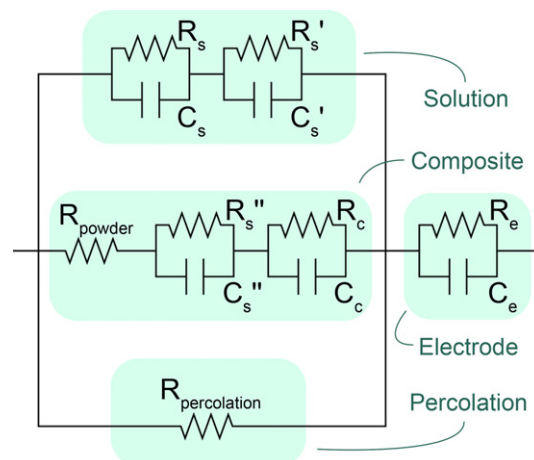
Fig. 3. Equivalent circuit model for powder-solution composite samples, with s representing solution, c representing particle-solution interfaces, and e representing the electrodes. R_{powder} represents particle resistance and $R_{percolation}$ accounts for the particle-to-particle current path.

sample geometry. Figure 4 presents results for (a) as-prepared, pure TiO_2 and (b) heat treated, Nb-substituted powders, which were representative of the results of all powder samples investigated. From these plots, it is apparent that at low $\sigma_{solution}$ the measured conductivity (open circles) approaches a plateau. This can best be explained by the particle-to-particle current percolation mechanism shown in Fig. 3, which is independent of the solution conductivity and becomes the dominant conduction path when the solution conductivity is low compared to that of the powder. Because this mechanism represents a parallel conduction path to the composite path, the measured conductivity ($\sigma_{measured}$) can be corrected to reflect only the current traveling through the solution and composite paths according to the following equation:

$$\sigma_{composite} = \sigma_{measured} - \sigma_{percolation} \tag{1}$$

The corrected composite conductivity is represented by the solid data points in Fig. 4. Note that $\sigma_{percolation}$, which was between 4 and 7×10^{-3} S/cm for the as-prepared and $0.1–0.25 \times 10^{-3}$ S/cm for the heat-treated samples, is only an "effective" conductivity because it does not take into account the much smaller area over which this mechanism occurs, which is determined by the contact area between adjacent particles rather than the entire area of the sample.

The true powder conductivity can be derived from the corrected $\sigma_{composite}$ values. $\sigma_{composite}$ represents the conductivity of a mixture of randomly arranged particles embedded in a conductive matrix. This is described by the Bruggeman asymmetric (BA) model[23]:

$$\frac{K_{composite} - K_{powder}}{K_{composite}^{1/3}(1 - K_{powder})} = (1 - f) \tag{2}$$

In this equation, $K_{composite}$ represents the ratio of the conductivity of the composite slurry to that of the corresponding NaCl solution ($\sigma_{composite}/\sigma_{solution}$); K_{powder} is the ratio of the powder and solution conductivities ($\sigma_{powder}/\sigma_{solution}$), and f is the volume fraction of particles in the composite, estimated by:

$$f = \frac{m}{\rho}\left(\frac{1}{\pi r^2 l}\right) \tag{3}$$

where m and ρ are the mass and theoretical density of the powder, r is the radius of the polyethylene tube, and l is the

Fig. 2. Nyquist plots of undoped, heat-treated TiO_2 when the the solution is (a) much more conductive than the powder and (b) much less conductive. Results were normalized to a 4 mm interelectrode spacing. Frequency values are indicated as $\log(v)$ (white squares).
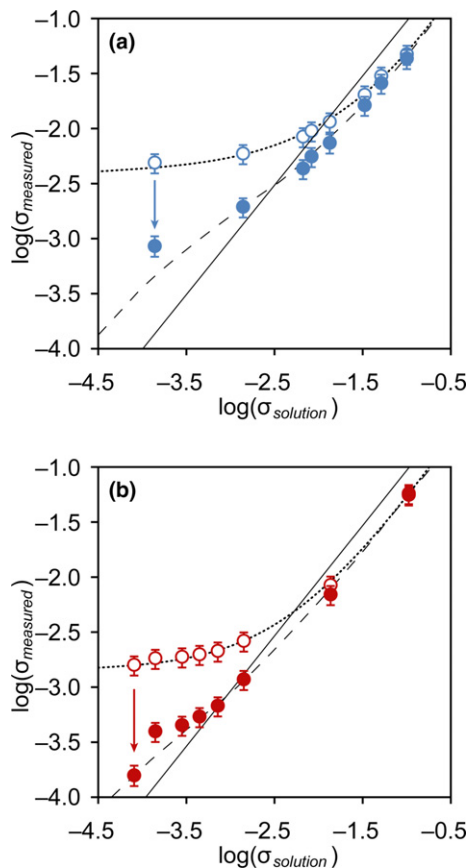
Fig. 4. Conductivity of powder-solution composites versus the corresponding solution conductivity for (a) as-prepared pure TiO$_2$ (blue circles) and (b) heat-treated, 0.6% Nb-substituted TiO$_2$ (red circles), as measured (open circles) and corrected to remove percolation effects (closed circles). The dashed line is the Bruggeman asymmetric model fit for the corrected conductivity.

interelectrode spacing. It can be seen that the BA model does a good job for solution conductivities greater than the "crossover point" in Figs. 4(a) and 4(b), i.e., the data points fall along the line predicted by this model running parallel to, but below the solution conductivity. For solution conductivities below the crossover point and corrected for particle percolation, the fit with the BA model line (parallel to and above the solution conductivity) is less satisfactory. We attribute this to uncertainty in the experimental data at low conductivities and in the subtraction process used to account for percolation.

The powder conductivity can be calculated from Eq. (2) using a single pair of composite and solution conductivity measurements. However, the uncertainty in individual measurements of conductivity (estimated to be 20%) and f can lead to very large errors in the calculated σ_{powder}. To minimize such uncertainties, Eq. (2) is used to fit the data for the entire range of solution conductivities. The powder conductivity is then represented by the "crossover" point in Fig. 4, where $\sigma_{composite} = \sigma_{solution} = \sigma_{powder}$. An uncertainty in this value of 40% was estimated by repeating the fitting procedure for the upper and lower limits of uncertainty in the individual data points.

The conductivity of each powder is summarized in Fig. 5. As expected for a donor-doped material, the conductivities of both as-prepared Nb^{5+}-substituted compositions are significantly higher than that of the pure TiO$_2$ powder (10×10^{-3} S/cm vs. 3×10^{-3} S/cm). In contrast, the conductivities determined for samples substituted with Ga^{3+} and Y^{3+} are within experimental uncertainty of the pure-TiO$_2$ conductivity. The behavior of the heat-treated powders is similar, although the 0.5% Nb-substituted specimen was not

significantly different from that of the pure-TiO$_2$ specimen. In addition, the conductivity of each powder decreased by approximately one order of magnitude upon heat treatment, which can be attributed to the increased oxygen concentration, measured by XPS in such heat-treated powders.[3] This suggests that the improvement in power conversion efficiency demonstrated by DSSCs containing Ga- and Y-substituted anatase is not caused by changes in the electrical conductivity.

The threefold increase in conductivity caused by Nb substitution may contribute to the modest performance improvement in Nb-substituted DSSCs. The relatively small magnitude of the conductivity change is somewhat surprising, however. If the majority of the Nb^{5+} ions were acting as donors, a conductivity increase of several orders of magnitude would be expected. Anatase prepared by other methods (e.g., thin film fabrication techniques) can be doped to such an extent, with correspondingly large increases in conductivity[2]; therefore, some characteristic of the hydrothermal synthesis technique must prevent dopant atoms from being effectively ionized. This low doping efficiency is also reflected in the lack of change in conductivity upon increasing the Nb content from 0.5% to 1%.

In the case of substitution by Y and Ga, which would act as acceptors if ionized, a decrease in n-type conductivity or even a changeover to p-type conductivity might be anticipated. Instead, there is no noticeable change in conductivity with doping, and DSSC properties indicate that these materials remain n-type.[5] This suggests the occurrence of ionic compensation by a donor species, such as oxygen vacancies (V$_O^{\bullet\bullet}$), known to form readily in TiO$_2$.[24] For example, a possible point defect reaction accounting for ionic compensation of Ga acceptors by oxygen vacancies would be:

$$Ga_2O_3 \xrightarrow{TiO_2} 2Ga'_{Ti} + 3O_O^{\times} + V_O^{\bullet\bullet} \tag{4}$$

A similar ionic compensation model can be described for Nb-substituted TiO$_2$. In this case, it is possible that the compensating defects are Ti^{3+} ions, which have been detected via XPS in hydrothermally synthesized anatase substituted with Nb.[3] A Ti^{3+} ion would be negatively charged relative to the normal Ti^{4+} site (Ti$_{Ti}'$). The compensation reaction can be written:
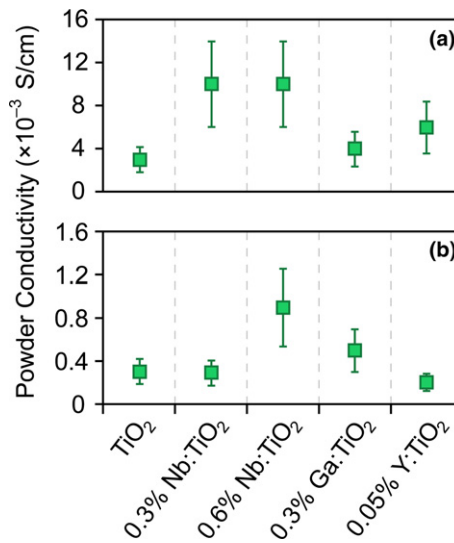
Fig. 5. Powder conductivities of (a) as-prepared and (b) heat-treated TiO$_2$ powders.

$$Nb_2O_5 + 2Ti^{\times}_{Ti} \xrightarrow{TiO_2} 2Nb^{\bullet}_{Ti} + 4O^{\times}_{O} + 2Ti'_{Ti} + \frac{1}{2}O_2(g) \qquad (5)$$

It is also conceivable that neutral defect clusters may form during hydrothermal synthesis, leading to a local compensation of either donor or acceptor impurities in anatase.

IV. Conclusions

Anatase titanium dioxide nanopowders have been synthesized using a hydrothermal synthesis route, both in pure form and with substitutional Nb^{5+}, Ga^{3+}, and Y^{3+}. The conductivity of each powder was measured using the PSC method to determine the extent to which conductivity changes with substitution. The PSC model was adjusted to account for the particle-to-particle current percolation observed in this system.

Substitution of Ti^{4+} by Nb^{5+} was shown to cause an increase in conductivity from 3×10^{-3} S/cm to 10×10^{-3} S/cm in as-prepared powders and 0.3×10^{-3} to 0.9×10^{-3} S/cm in heat-treated (520°C, 1 h) powders. This is a much smaller change than that observed in thin films of anatase doped with a similar amount of Nb, which we attribute to compensation by ionic defects. Ga^{3+} and Y^{3+} substitution had no measurable effect on the powder conductivity, which can also be explained by ionic compensation during powder synthesis.

Although small compared to thin film results, the conductivity increase observed upon addition of Nb is detectable and may be a factor in the improved device performance of Nb-substituted DSSCs based upon hydrothermally synthesized powders. It should be noted, however, that conductivity is a product of carrier content and mobility, which we cannot deconvolute based upon PSC measurements. High mobilities may be a contributing factor in DSSC performance. On the other hand, the lack of conductivity improvement with Ga- and Y- substitution suggests that factors other than conductivity (e.g., surface segregation, surface transfer reactions, etc.) are responsible for the improved performance of DSSCs substituted with these species.

References

[1] A. Fujishima and K. Honda, "Electrochemical Photolysis of Water at a Semiconductor Electrode," *Nature*, **238**, 37–8 (1972).
[2] Y. Furubayashi, T. Hitosugi, Y. Yamamoto, Y. Hirose, G. Kinoda, K. Inaba, T. Shimada, and T. Hasegawa, "Novel Transparent Conducting Oxide: Anatase $T_{1-x}Nb_xO_2$," *Thin Solid Films*, **496**, 157–9 (2006).
[3] A. K. Chandiran, F. Sauvage, M. Casas-Cabanas, P. Comte, S. M. Zakeeruddin, and M. Graetzel, "Doping a TiO_2 Photoanode with Nb^{5+} to Enhance Transparency and Charge Collection Efficiency in Dye-Sensitized Solar Cells," *J. Phys. Chem. C*, **114**, 15849–56 (2010).
[4] B. O'Regan and M. Grätzel, "A low-Cost, High-Efficiency Solar Cell Based on Dye-Sensitized Colloidal TiO_2 Films," *Nature*, **353**, 737–40 (1991).
[5] A. K. Chandiran, F. Sauvage, L. Etgar, and M. Graetzel, "Ga^{3+} and Y^{3+} Cationic Substitution in Mesoporous TiO_2 Photoanodes for Photovoltaic Applications," *J. Phys. Chem. C*, **115**, 9232–40 (2011).
[6] K. Zhu, N. Kopidakis, N. R. Neale, J. van de Lagemaat, and A. J. Frank, "Influence of Surface Area on Charge Transport and Recombination in dye-Sensitized TiO_2 Solar Cells," *J. Phys. Chem. B*, **110**, 25174–80 (2006).
[7] B. C. O'Regan, J. R. Durrant, P. M. Sommeling, and N. J. Bakker, "Influence of the $TiCl_4$ Treatment on Nanocrystalline TiO_2 Films in Dye-Sensitized Solar Cells. 2. Charge Density, Band Edge Shifts, and Quantification of Recombination Losses at Short Circuit," *J. Phys. Chem. C*, **111**, 14001–10 (2007).
[8] M. Grätzel, "Recent Advances in Sensitized Mesoscopic Solar Cells," *Acc. Chem. Res.*, **42**, 1788–98 (2009).
[9] A. K. Ghosh and H. P. Maruska, "Photoelectrolysis of Water in Sunlight with Sensitized Semiconductor Electrodes," *J. Electrochem. Soc.*, **124**, 1516 (1977).
[10] H. P. Maruska and A. K. Ghosh, "Transition-Metal Dopants for Extending the Response of Titanate Photoelectrolysis Anodes," *Sol. Energ. Mater.*, **1**, 237–47 (1979).
[11] C. Stalder and J. Augustynski, "Photoassisted Oxidation of Water at Beryllium-Doped Polycrystalline TiO_2 Electrodes," *J. Electrochem. Soc.*, **126**, 2007 (1979).
[12] R. D. Shannon, "Revised Effective Ionic Radii and Systematic Studies of Interatomic Distances in Halides and Chalcogenides," *Acta Crystallogr. A*, **A32**, 751 (1976).
[13] T. Hitosugi, H. Kamisaka, K. Yamashita, H. Nogawa, Y. Furubayashi, S. Nakao, N. Yamada, A. Chikamatsu, H. Kumigashira, M. Oshima, Y. Hirose, T. Shimada, and T. Hasegawa, "Electronic Band Structure of Transparent Conductor: Nb-Doped Anatase TiO_2," *Appl. Phys. Express*, **1**, 111203 (2008).
[14] J. Augustynski, J. Hinden, and C. Stalder, "Novel Semiconducting Electrodes for Photosensitized Electrolysis of Water," *J. Electrochem. Soc.*, **124**, 1063–4 (1977).
[15] J. F. Houlihan, D. B. Armitage, T. Hoovler, and D. Bonaquist, "Doped Polycrystalline TiO_2 Electrodes for Photo-Assisted Electrolysis of Water," *Mater. Res. Bull.*, **13**, 1205–12 (1978).
[16] J. Li, X. Yang, X. Yu, L. Xu, W. Kang, W. Yan, H. Gao, Z. Liu, and Y. Guo, "Rare Earth Oxide-Doped Titania Nanocomposites with Enhanced Photocatalytic Activity Towards the Degradation of Partially Hydrolysis Polyacrylamide," *Appl. Surf. Sci.*, **255**, 3731–8 (2009).
[17] S. M. Zakeeruddin and M. Grätzel, "Solvent-Free Ionic Liquid Electrolytes for Mesoscopic Dye-Sensitized Solar Cells," *Adv. Funct. Mater.*, **19**, 2187–202 (2009).
[18] I. K. Ding, N. Tetreault, J. Brillet, B. E. Hardin, E. H. Smith, S. J. Rosenthal, F. Sauvage, M. Graetzel, and M. D. McGehee, "Pore-Filling of Spiro-OMeTAD in Solid-State Dye Sensitized Solar Cells: Quantification, Mechanism, and Consequences for Device Performance," *Adv. Funct. Mater.*, **19**, 2431–6 (2009).
[19] Y. Chiba, A. Islam, R. Komiya, N. Koide, and L. Y. Han, "Conversion Efficiency of 10.8% by a Dye-Sensitized Solar Cell Using a TiO_2 Electrode with High Haze," *Appl. Phys. Lett.*, **88**, 223505 (2006).
[20] B. J. Ingram and T. O. Mason, "Powder-Solution-Composite Technique for Measuring Electrical Conductivity of Ceramic Powders," *J. Electrochem. Soc.*, **150**, E396–402 (2003).
[21] Q. Wang, G. Lian, and E. C. Dickley, "Grain Boundary Segregation in Yttrium-Doped Polycrystalline TiO_2," *Acta Mater.*, **52**, 809–20 (2004).
[22] A. Ahmad, S. Buzby, C. Ni, and S. I. Shah, "Effect of Nb and Sc Doping on the Phase Transformation of Sol-gel Processed TiO_2 Nanoparticles," *J. Nanosci. Nanotechnol.*, **8**, 2410–8 (2008).
[23] R. E. Meredith and C. W. Tobias, *Advances in Electrochemistry and Electrochemical Engineering*. Interscience, New York, 1962.
[24] A. Weibel, R. Bouchet, and P. Knauth, "Electrical Properties and Defect Chemistry of Anatase (TiO_2)," *Solid State Ionics*, **177**, 229–36 (2006). □